Pergamon

Atmospheric Environment Vol. 28, No. 7, pp. 1327–1338, 1994

1352-2310/94 $6.00+0.00

MODELING COAGULATION AMONG PARTICLES OF DIFFERENT COMPOSITION AND SIZE

MARK Z. JACOBSON and RICHARD P. TURCO

Department of Atmospheric Sciences, 405 Hilgard Ave., University of California, Los Angeles, CA 90024-1565, U.S.A.

and

ERIC J. JENSEN and OWEN B. TOON

Space Science Division, NASA Ames Research Center, Moffett Field, CA 94035-1000, U.S.A.

(*First received* 23 *May* 1993 *and in final form* 10 *October* 1993)

Abstract—We present a technique for simulating coagulation among any number of aerosol types, each with a different composition. The semi-implicit solution mechanism solves the coagulation equations over size ranges divided into any number of discrete bins. The scheme conserves particle volume, requires no iterations, and is numerically stable, regardless of the time-step. We compared the accuracy of the solution to both analytical and time-series numerical solutions. Practical use of the scheme demonstrates that it is computationally fast in a multiple grid-cell model.

Key word index: Aerosol microphysics, multicomponent aerosols, atmospheric modeling, semi-implicit solutions.

1. INTRODUCTION

Aerosol coagulation is important because it alters the composition and size distribution of particles primarily smaller than one micron in diameter, and these particles affect visibility, health, and physical processes in the atmosphere. For example, sulfate, nitrate, and organic carbon particles between 0.2 and 1.0 μm in diameter scatter light, and soot particles smaller than 1.0 μm absorb light efficiently (Waggoner *et al.*, 1981; Ouimette and Flagan, 1982). Also, particles between 0.1 and 1.0 μm penetrate to the deepest parts of human lungs. Finally, small particles serve as cloud condensation nuclei and surfaces on which chemical reactions take place, and small aqueous particles absorb gases and serve as hosts for internal chemical reactions.

Simulating coagulation requires computing collision and coalescence rates and changes in particle size and composition over time. Atmospheric particles collide as a result of Brownian motion, differences in fall velocities, turbulent motions, and intraparticle forces. Generally, Brownian motion affects particles smaller than 1 μm in diameter, differential fall velocities and turbulent motions affect particles larger than 1 μm, and intraparticle forces affect particles independently of size (Fuchs, 1964).

Smoluchowski (1918) calculated an expression for the coagulation *kernel* associated with Brownian motion in the continuum regime, where the Knudsen number (Kn) is much less than unity. In the free molecular regime ($Kn > 1$), the Brownian coagulation kernel appears to follow the kinetic theory of binary collisions for gas molecules (Hidy and Brock, 1970; Hirschfelder *et al.*, 1951). Fuchs (1964) developed an interpolation formula, described in Section 3.3, for the Brownian kernel in the transition regime ($0.1 < Kn < 10$). Fuchs' kernel matches the continuum value at low Knudsen number and the free molecular value at high Knudsen number (see also Sitarski and Seinfeld, 1977).

To simulate changes in the size distribution of coagulating aerosols, modelers have developed a number of approaches that assume either a continuous size spectrum or discrete bins that vary in size (e.g. Lushnikov, 1975; Turco *et al.*, 1979a,b; Suck and Brock, 1979; Gelbard and Seinfeld, 1980; Tsang and Brock, 1982; Seigneur, 1982; Friedlander, 1983; Warren and Seinfeld, 1985; Toon *et al.*, 1988; Kim and Seinfeld, 1990; Strom *et al.*, 1992). While all of these models simulate changes in size of coagulating particles, few calculate changes in composition of such particles, and fewer calculate changes in size and composition among different types of particles, each with a different composition.

In one such case Turco *et al.* (1979a,b) derived a basic semi-implicit algorithm to describe aerosol droplets coagulating with condensation nuclei to form mixed aerosols. Their equations assumed a geometrically related size distribution, with the volume ratio of adjacent size bins equal to two. Toon *et al.* expanded this semi-implicit technique to allow the fixed volume ratio between adjacent bins to exceed two. Here, we further develop the coagulation equations to allow the volume ratio of adjacent bins to approach unity. Furthermore, while we show results using a geometric size distribution, the method presented here solves over randomly spaced size bins as

well. Finally, the scheme simulates coagulation among any number of particle types, each containing any number of volume fraction components.

2. TYPES AND SIZES OF AEROSOLS SIMULATED

The size-resolved model we present simulates coagulation over any number of *externally mixed* (EM) particle types and a single *internally mixed* (IM) type. EM types can contain any number of *volume fractions* (EMVFs). Examples of EM particles with one volume fraction are those containing only elemental carbon, organic carbon, or dust. An example of EM particles with two volume fractions are those containing sulfuric acid and water.

The internally mixed particle type can also contain any number of volume fractions (IMVFs), but must contain at least the sum of the number of volume fractions in EM types. For example, if we have one EM type with one volume fraction and another with two volume fractions, then we require at least three IMVFs because coagulation of the two EM types results in IM particles containing three components. The IM type, however, can contain any number of volume fractions beyond the minimum number. Examples of such additional components are condensed liquids, dissociated ions, aqueous chemistry by-products, emitted species, or background species. We can have more than one IM type; however, each IM type must contain all components in the system. For simplicity, we discuss modeling a single IM type in this paper.

The term, "internally mixed" as used here, does not necessarily mean that the components are well-mixed in solution. It merely means that the components exist together in the same particle, possibly even in different phases (e.g. liquid and solid). Some of the components may be well-mixed in solution, but others may not be. The only difference between "externally mixed" and "internally mixed" particles, as defined here, is that the IM particles must contain at least the number of components in all the EM particles, combined. Figure 1 shows an example of the particle types, and Table 1 shows the intended effect of different-type particles coagulating.

Among the assumptions we make is that when an EM particle *hetero-coagulates* (e.g. an EM particle coagulates with any particle except an EM of the same type), then the resulting particle enters a multicomponent mixture (IM) representing all particle types. In reality, when two particles of different composition collide, they form a third particle of unique composition. However, while we can write the equations to solve for every combination of particles, modeling every combination is computationally impractical beyond a small number of particles and spatial grid-cells. For example, if we initially have 11 distinct particle types, then they will coagulate into 2047 mixtures (the sum of combinations of 11 taken $1, 2, \ldots, 11$ at a time). If we distribute 72 volume fractions (typical of an air pollution model we currently run) among the 11 types, then each of the 2047 combinations will have between one and 72 components. In a model with 30 size bins and 10,000 grid-cells, we would track 12.3 billion pieces of information each time-step if the average combined species had 20 components. The memory requirements for such a model are beyond most current computer capabilities.

However, by assuming that EM particles become IM particles when they hetero-coagulate, we reduce the number of resulting particle types in the above

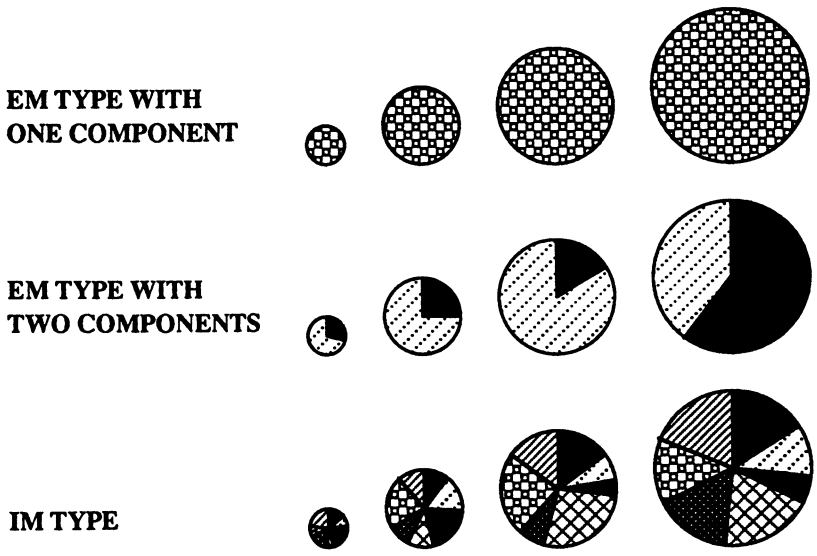

Fig. 1. Simplified example of particle types in the model. Externally mixed (EM) types can contain one or more volume fraction components and the single internally mixed (IM) type contains at least the number of EM components but can also contain any number of additional components.

Table 1. The intended effects on number and volume concentrations when particles of one type coagulate with particles of either the same or another type. EM1 is one set of externally mixed particles, EM2 is another set, IM is the internally mixed type, EMVF1s and EMVF2s are volume fractions of EM1 and EM2, respectively, and IMVFs are volume fractions of the IM type. A (−) indicates a decrease in either number of volume, a (+) indicates an increase, a (0) indicates no change, and a (—) indicates that no effect is applicable. For example, when EM coagulate with IM particles, EM particles decrease and IM particles increase in number and volume, and volume fractions of EM particles transfer to IM particles

	Number			Volume					
Coagulating pairs	EM1	EM2	IM	EM1	EMVF1	EM2	EMVF2	IM	IMVF
EM1 w/EM1	(−)	—	—	(0)	(0)	—	—	—	—
EM1 w/EM2	(−)	(−)	(+)	(−)	(−)	(−)	(−)	(+)	(+)
EM1 w/IM	(−)	—	(0)	(−)	(−)	—	—	(+)	(+)
IM w/IM	—	—	(−)	—		—	—	(0)	(0)

case from 2047 to 12. With 86 total elements (e.g. 10 EM types with one volume fraction each, one EM with two volume fraction, and one IM with 72 volume fractions) the model would track 25.8 million pieces of information over the 10,000-cell grid-domain, which is a factor of 500 savings in array space. Thus, while we can code all possible particle combinations, the computer memory requirements in a three-dimensional model are prohibitively large, and our assuming that different-type particles coagulate to a single IM type is more practical, although less ideal.

3. SOLUTIONS TO THE COAGULATION EQUATION

3.1. *Semi-implicit solution for particles of uniform composition*

We first derive the semi-implicit solution to the coagulation equation for particles of uniform composition and later expand the derivation to particles of different composition. To derive the semi-implicit solution, we start with the integro-differential equation (Muller, 1928)

$$\frac{\partial C_v}{\partial t}=\frac{1}{2}\int_0^v \beta_{v-\bar{v},\bar{v}} C_{v-\bar{v}} C_{\bar{v}}\,\mathrm{d}\bar{v} - C_v\int_0^\infty \beta_{v,\bar{v}} C_{\bar{v}}\,\mathrm{d}\bar{v} \tag{1}$$

where C is the time-dependent number concentration (No. cm^{-3}) of particles of volume v, $v-\bar{v}$, or $\bar{v}$, and β is the coagulation kernel (cm^{-3} No.$^{-1}$ s^{-1}) of two colliding particles. For size bins consisting of monomers (e.g. the volume of bin k equals $k\times$ the volume of bin one), we rewrite equation (1) as

$$\frac{\partial C_k}{\partial t}=\frac{1}{2}\sum_{j=1}^{k-1}\beta_{k-j,j}C_{k-j}C_j - C_k\sum_{j=1}^{\infty}\beta_{k,j}C_j \tag{2}$$

where we substituted the volume subscripts in equation (1) with the size-bin subscripts in equation (2).

The next step in the derivation of the semi-implicit solution is to write equation (2) in fully implicit finite difference form as

$$C_k^{t+1}=C_k^t+\frac{1}{2}\Delta t\sum_{j=1}^{k-1}P_{k,j}-\Delta t\sum_{j=1}^{\infty}L_{k,j} \tag{3}$$

where Δt is the time-step (s), superscripts t and $t+1$ indicate initial and final concentrations, respectively, while

$$P_{k,j}=\beta_{k-j,j}C_{k-j}^{t+1}C_j^{t+1} \tag{4}$$

and

$$L_{k,j}=\beta_{k,j}C_k^{t+1}C_j^{t+1} \tag{5}$$

are production and loss rates (No. cm^{-3} s^{-1}), respectively.

Third, to obtain the semi-implicit solution, we redefine the loss term from equation (5) in semi-implicit form as

$$L_{k,j}=\beta_{k,j}C_k^{t+1}C_j^t. \tag{6}$$

Using equation (6) instead of equation (5) will allow a non-iterative solution to coagulation that approximates an exact solution. Equations (4) and (5) require that $P_{k,j}=L_{k-j,j}$ for each k and j. Applying this equality to equation (6) and plugging the result and equation (6) into equation (3), we obtain the semi-implicit coagulation solution for monomer particles of uniform composition as

$$C_k^{t+1}=\frac{C_k^t+\frac{1}{2}\Delta t\sum_{j=1}^{k-1}\beta_{k-j,j}C_{k-j}^{t+1}C_j^t}{1+\Delta t\sum_{j=1}^{\infty}\beta_{k,j}C_j^t}. \tag{7}$$

where k varies from one to infinity. While equation (7) correctly accounts for the reduction in particle number when two particles coagulate (reducing the number by one-half), it does not conserve volume (equation (3) correctly accounts for both number and volume, but is fully implicit). In order to conserve volume (which coagulation physically does) while giving up some accuracy in number, we reform equation (7) as

$$v_kC_k^{t+1}=\frac{v_kC_k^t+\Delta t\sum_{j=1}^{k-1}\beta_{k-j,j}v_{k-j}C_{k-j}^{t+1}C_j^t}{1+\Delta t\sum_{j=1}^{\infty}\beta_{k,j}C_j^t}. \tag{8}$$

Equation (8) satisfies the volume-conservation requirement, $v_{k-j}P_{k,j}=v_{k-j}L_{k-j,j}$, for each k and j.

While equation (8) solves the equation over a monomer size-bin structure, we wish to solve it over different bin structures. For example, suppose we set up geometric bins, where the volume of one bin equals the volume of the previous bin multiplied by a constant factor. In this particular distribution, the volume of the smallest bin is $v_1=(4/3)\pi(r_1)^3$, where r_1 is the radius of the smallest bin. Furthermore $V_{RAT}=v_{i+1}/v_i$ is the volume ratio of two adjacent bins and N_B is the total number of size bins. For any value of V_{RAT} greater than one, the volume of bin i is

$$v_i=v_1V_{RAT}^{i-1} \tag{9}$$

and the radius is

$$r_i=r_1V_{RAT}^{(i-1)/3}. \tag{10}$$

Consequently, the number of bins that covers the particle size range from radius r_1 to r_i is

$$i=1+\ln[(r_i/r_1)^3]/\ln[V_{RAT}]. \tag{11}$$

Thus, for a radius from 0.01 μm (10^{-6} cm) to 1 mm (10^{-1} cm), the model requires 87 ($=N_B$) bins when $V_{RAT}=1.5$ and 26 bins when $V_{RAT}=4$.

With this new bin structure, each time a model particle of size i collides and sticks to a model particle of size j, the resulting volume of the intermediate particle is

$$V_{i,j}=v_i+v_j. \tag{12}$$

The intermediate particle has volume between those of two model bins, k and $k+1$. We partition the intermediate particle between the two bins by defining $f_{i,j,k}$, the volume fraction of intermediate particles of size $V_{i,j}$ that we partition to each model bin k. More precisely

$$f_{i,j,k}=\begin{cases}\left(\dfrac{v_{k+1}-V_{i,j}}{v_{k+1}-v_k}\right)\dfrac{v_k}{V_{i,j}} & v_k\leqslant V_{i,j}<v_{k+1};\quad k<N_B\\ 1-f_{i,j,k-1} & v_{k-1}<V_{i,j}<v_k;\quad k>1\\ 1 & V_{i,j}\geqslant v_k;\quad k=N_B\\ 0 & \text{all other cases}\end{cases}. \tag{13}$$

The fractions in equation (13) are independent of the size-bin structure. Thus, they work with monomer structures (where all values of f would be 1 or 0), geometric structures, or random structures. Applying the fractions in equations (13)–(8), we obtain the general formula for volume-conserving, semi-implicit coagulation for particles of uniform composition as

$$v_kC_k^{t+1}=\frac{v_kC_k^t+\Delta t\sum_{j=1}^{k}\left\{\sum_{i=1}^{k-1}f_{i,j,k}\beta_{i,j}v_iC_i^{t+1}C_j^t\right\}}{1+\Delta t\sum_{j=1}^{N_B}\left(1-f_{k,j,k}\right)\beta_{k,j}C_j^t}. \tag{14}$$

In equation (14), values for $f_{i,j,k}$ are frequently zero; thus, to speed the computer solution to equation (14), we eliminate every multiplication by a zero value of f. Also in equation (14) each C^{t+1} term on the right-hand side of the equation is a final concentration calculated for a previous bin. No production occurs in the first bin, $k=1$, since $k-1=0$ in equation (14). Thus all C_i^{t+1} terms are known when calculating C_k^{t+1}.

The advantage of using a semi-implicit equation. such as equations (7), (8), or (14) instead of a fully implicit equation, such as equation (2), is significant. For example, equations (7), (8), and (14) allow immediate, volume-conserving solutions, using any time-step. A solution to equation (2), on the other hand, requires the use of an ordinary differential equation solver, which performs iterations. The only disadvantage to equations (8) and (14) is that, as with most other schemes, particle number is not exactly accounted for. However, by increasing the resolution of the bin structure (e.g. by decreasing V_{RAT}), the error in number approaches zero (e.g. Section 4) while the solution remains non-iterative and volume conserving.

3.2. *Semi-implicit solution for particles of different type and composition*

The coagulation equations for particles of different type and composition are similar to those for particles of uniform composition. However, because the variety of particle types in the more complicated case can cause confusion, we present a simplified scenario and some definitions in the Appendix.

As discussed earlier, the particle types we use are externally mixed (EM) and internally mixed (IM). We first solve for the final concentration of all components in EM types by marching from bin $k=1$ through bin $k=N_B$. EM types lose volume by coagulating either with other EM types or with the IM type. When such heterogeneous loss occurs, the IM type gains volume. When EM particles self-coagulate, their volume shifts to larger particles of the same type; thus, volume does not escape to the IM type. In sum, for each $N=1$, N_E EM type and each $U=1$, T_N component, where $Q=L_{N,U}$ is the component number (terms defined in Appendix), the final concentration in each

bin is

$$v_k C_{Qk}^{t+1} = \frac{v_k C_{Qk}^t + \Delta t \sum_{j=1}^{k} \left(\sum_{i=1}^{k-1} f_{i,j,k} \beta_{Ni,Nj} v_i C_{Qi}^{t+1} C_{LN,ij}^t \right)}{1 + \Delta t \sum_{j=1}^{N_B} \left\{ (1 - f_{k,j,k}) \beta_{Nk,Nj} C_{LN,ij}^t + \sum_{\substack{M=1 \\ M \neq N}}^{N_T} \beta_{Nk,Mj} C_{LM,ij}^t \right\}}. \quad (15)$$

Thus, equation (15) accounts for homogeneous production and loss and heterogeneous coagulation loss of EM particles. No production occurs into the first bin of EM types. In equation (15), β is the coagulation kernel. However, the subscripts refer to particles of different types. For example, $\beta_{Nk,Mj}$ indicates the rate that a particle of bin k, type N (an EM) coagulates with a particle of bin j, type M (either a different EM, or the IM).

After solving for concentrations of EM components, we solve for those of IM particles. IM particles gain volume when EM particles coagulate with them or when EM particles coagulate with EM particles of another type. IM particles never lose volume through coagulation; however, volume shifts to higher bins upon hetero- or self-coagulation. To solve for IM concentrations, we march from bin $k=1$ through bin $k=N_B-1$ (we do not allow IM particles to lose volume from the largest size-bin but we allow heterogeneous production into the first bin of IM particles). For the single $N=N_T$ IM type and each $U=1$, T_N component of the IM type, where $Q=L_{N,U}$, the final concentration is

$$v_k C_{Qk}^{t+1} = \frac{v_k C_{Qk}^t + \Delta t \sum_{M=1}^{N_T} \sum_{j=1}^{k} C_{LM,ij}^t \sum_{i=1}^{k-1} f_{i,j,k} \beta_{Ni,Mj} v_i C_{Qi}^{t+1} + \sum_{\substack{I=1 \\ I \neq M \\ S_{Q,I}>0}}^{N_E} \sum_{i=1}^{k} f_{i,j,k} \beta_{Ii,Mj} v_i C_{S_{Q,I}i}^{t+1}}{1 + \Delta t \sum_{\substack{M=1 \\ K \neq N_B}}^{N_T} \left\{ \sum_{j=1}^{N_B} (1 - f_{k,j,k}) \beta_{Nk,Mj} C_{LM,ij}^t \right\}} \quad (16)$$

where the Appendix defines the subscript array $S_{Q,I}$. As in equations (14) and (15), equation (16) contains many values of f that are zero. Each computation with such a value should be eliminated. For a single particle type of uniform composition, equation (15) disappears ($N_E=0$) and equation (16) simplifies to equation (14).

Thus, equations (15) and (16) define the generalized, volume-conserving, semi-implicit coagulation equations for multicomponent, multi-type aerosols. To conserve volume at the boundary, equation (16) assumes that particles cannot coagulate out of the largest size bin of IM particles. They can, however, coagulate from the largest EM particles to become IM particles. The equations also assume that, upon hetero-coagulation, all volume goes to IM particles. To change this assumption so that when particles hetero-coagulate, they produce a new mixture, we only need to define the new particle types and shift the heterogeneous production term from equation (16) to the equation for the new particle types. The new equation will also contain a homogeneous coagulation production term, a homogeneous loss term, and a heterogeneous loss term, all similar to those in equation (15).

3.3. *Coagulation kernel*

For part of this work, we calculated the coagulation kernel by assuming only Brownian diffusion. However, empirical equations in Pruppacher and Klett (1978) describe additional coagulation rates, including those for convective diffusion enhancement, gravitation, turbulent shear, and turbulent inertial motion (see also Saffman and Turner (1956) for coagulation rates due to turbulent shear and inertial motion). To calculate the Brownian diffusion kernel ($\beta_{i,j}^B$ — $\mathrm{cm^3\ No.^{-1}\ s^{-1}}$) we used Fuchs' (1964) interpolation formula

$$\beta_{i,j}^B = \frac{4\pi(r_i + r_j)(D_i + D_j)}{\dfrac{r_i + r_j}{r_i + r_j + (\delta_i^2 + \delta_j^2)^{1/2}} + \dfrac{4(D_i + D_j)}{(\bar{v}_{pi}^2 + \bar{v}_{pj}^2)^{1/2}(r_i + r_j)}} \quad (17)$$

where r_i and r_j are the radii (cm) of particles i and j, respectively. Also, D_i (or D_j) is the particle diffusion coefficient ($\mathrm{cm^2\ s^{-1}}$) defined as

$$D_i = \frac{k_B T}{6\pi r_i \eta} \left\{ 1 + Kn_i \left[A + B \exp\left(-CKn_i^{-1} \right) \right] \right\} \quad (18)$$

which simplifies to the Stokes–Einstein formula in the continuum regime ($Kn_i \ll 1$). In equation (18), $Kn_i = \lambda_g / r_i$ is the Knudsen number of particle i, k_B is Boltzmann's constant, T is the temperature (K), η is the dynamic viscosity of air, and A, B, and C are corrections for particle resistance to motion (see Millikan, 1923). We normally use the values $A=1.249$, $B=0.42$, and $C=0.87$, suggested by Kasten (1968).

In addition, the mean free path ($\mathrm{cm\ s^{-1}}$) of a gas molecule is

$$\lambda_g = \frac{2\eta}{\rho_g \bar{v}_g} \quad (19)$$

where ρ_g is the density of air, and $\bar{v}_g$ is the mean thermal velocity of an air molecule. The thermal velocity of an air molecule is similar to that of a particle of size i

$$\bar{v}_g \quad \text{or} \quad \bar{v}_{pi}=\left(\frac{8k_BT}{\pi m_i}\right)^{1/2} \tag{20}$$

except that, for a particle of size i, m_i is the mass of the particle, and for an air molecule, m_i is the mass of the air molecule. Finally, Fuchs defined the mean distance from the center of a sphere reached by particles leaving the surface of the sphere and traveling a distance of particle mean free path λ_{pi} as

$$\delta_i=\frac{\{(2r_i+\lambda_{pi})^3-(4r_i^2+\lambda_{pi}^2)^{3/2}\}}{6r_i\lambda_{pi}}-2r_i \tag{21}$$

where

$$\lambda_{pi}=\frac{8D_i}{\pi\bar{v}_{pi}}. \tag{22}$$

In the continuum regime, equation (17) simplifies to its numerator, while in the free molecular regime ($Kn_i \gg 10$) it simplifies to

$$\beta^B_{i,j}=\pi(r_i+r_j)^2(\bar{v}_{pi}^2+\bar{v}_{pj}^2)^{1/2}. \tag{23}$$

4. TESTS OF THE ALGORITHM

To demonstrate the basic features of the coagulation solution scheme, we present tests against Smoluchowski's analytical solution, two numerical solutions, an analytical solution to a self-preserving distribution, and a published comparison. In the first test, we compared our semi-implicit coagulation solution to the analytical solution of Smoluchowski (1918—see also Hidy and Brock, 1970; Seinfeld, 1986). Smoluchowski's solution applies to an initial distribution where all particles are of uniform size (monodisperse) and composition, and where the coagulation kernel (β) is constant for all interactions. The monodisperse distribution is the narrowest possible distribution. The size-bin grid use for Smoluchowski's solution has a monomer structure (as discussed earlier), which is arranged so that the volume of the kth bin equals k multiplied by the volume of the first ($k=1$) bin. Given an initial number concentration C^t in the first bin, Smoluchowski predicted that the concentration at any time $t+1$ (or $t+\Delta t$) in bin k is

$$C_k^{t+1}=\frac{C^t(0.5\beta C^t\Delta t)^{k-1}}{(1+0.5\beta C^t\Delta t)^{k+1}}. \tag{24}$$

Using a constant $\beta=8k_BT/3\eta$ and an initial number concentration of $10^6\,\text{cm}^{-3}$, we compared Smoluchowski's solution to our solution after a 12 h simulation period (Fig. 2). For the semi-implicit scheme, we calculated one case with $V_{RAT}=1.2$ (39 bins per decade), another with $V_{RAT}=1.5$ (18 bins per decade), and a third with $V_{RAT}=2$ (11 bins per decade). Because the semi-implicit and analytical solutions extend over bin-widths of different sizes, we divided the number concentrations in Fig. 2 by $d\log D_p$ to normalize them. Also, for the geometric size grid, when $V_{RAT}<1.62$ and particles in the first bin coagulate with particles in the second bin, the resulting particles are larger than the third bin. Thus, a dip will occur in the concentration of the second bin. To remedy this, we made the volume of the second bin equal to two times the volume of the first bin ($V_{RAT}=2$ for the second bin only), which is the same ratio as that between the first and second bin of the monomer structure. Since the semi-implicit solution is independent of the bin structure, the modification to the second bin when $V_{RAT}<1.62$ requires no other changes.

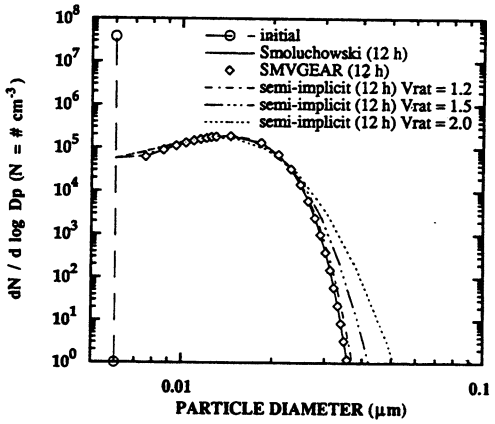

Fig. 2. Comparison of semi-implicit and integrated coagulation results to Smoluchowski's analytical solution. The coagulation period was 12 h, the initial distribution was monodisperse, and the coagulation kernel was constant. For each of the three semi-implicit cases ($V_{RAT}=1.2$, 1.5 and 2.0), the time-step was 600 s. We used SMVGEAR to solve 1000 equations and unknowns to produce an integrated solution to equation (2) for 1000 monomer size-bins. The first bin for the Smoluchowski and SMVGEAR solutions were omitted from the graph since the lower bin diameter in both cases was zero, making $d\log D_p$ infinite.

Figure 2 also shows a solution to this monodisperse initial distribution generated by SMVGEAR, a Gear-type solver of ordinary differential equations (Jacobson and Turco, 1994). With SMVGEAR, we solved equation (2) simultaneously for 1000 monomer size bins. Equation (2) applied to the given bin structure resulted in a non-sparse matrix of partial derivatives with order 1000. Since 1000 monomer bins covers only one decade in radius space and the matrix of partial derivatives has no sparsity, we conclude that solving the monomer structure with an integrator is inefficient for atmospheric models. However, as Fig. 2 shows SMVGEAR provided an exact solution to this problem.

By comparison, the semi-implicit method gave solutions that approached the analytical solution as V_{RAT} decreased. At $V_{RAT}=1.2$, the semi-implicit solution almost matched the exact solution for the full range of sizes shown, while for larger values of

V_{RAT} and large diameters, numerical diffusion increased. To obtain the semi-implicit solutions, we took a series of 600-s time-steps during the 12-h simulation period. Using a larger (e.g. 3 h) or smaller (e.g. 60 s) time-step hardly changed the results. For example, with $\Delta t = 3$ h and $V_{RAT} = 1.2$, the semi-implicit solution resulted in less numerical diffusion than it did with $\Delta t = 600$ and $V_{RAT} = 1.5$. Thus, the time-step had a smaller effect on numerical diffusion than did the size bin resolution. Finally, the semi-implicit solution exactly conserved volume in all cases. As V_{RAT} decreased, bin resolution increased, and the total number concentration of particles approached the correct value. This held true for all the cases tested in Figs 2–4.

In the second and third tests, we compared two time-series of semi-implicit solutions against those of integrated solutions. For these results, we started with initial lognormal distributions, both with mean diameter 0.02 μm and number concentration of 10^6 cm^{-3}. In one case (Fig. 3a) the initial geometric standard deviation was 1.4, and in the other (Fig. 3b), the deviation was 1.15. We integrated equation (2) with SMVGEAR, using 5500 monomer size bins for Fig. 3a and 2000 bins for Fig. 3b. In both cases, we solved the semi-implicit equations using $V_{RAT} = 1.2$, 1.5, and 2.0. However, Figs 3a and 3b show only the $V_{RAT} = 1.2$ time-series solutions. In both cases, the figures show that the semi-implicit solutions followed the integrated solutions almost exactly at each of the 2-, 4-, and 6-h marks. Again, we used a 600-s time-step for the semi-implicit solutions. A larger or smaller time-step hardly changed the results. However, increasing V_{RAT} increased numerical diffusion at higher diameters, although not so much as in Fig. 2.

For the conditions of Figs 2, 3a, and 3b, the characteristic time for coagulation, $\tau = 2/\beta C^t$, was less than 1 h. Thus, the time intervals used (6–12 h) were reasonably long enough to test for numerical diffusion.

In the fourth test, we compared the semi-implicit scheme to an analytical solution of a self-preserving distribution described in Seinfeld (1986). For this solution, the initial number density, C^t, of a uniform aerosol was spread exponentially about bin $i = p$, where v_p is the volume of bin p. At any time t, coagulation changed the number concentration in size bin i to

$$C_i^{t+1} = \frac{C^t dv_i/v_p}{(1+0.5\beta C^t \Delta t)^2} \exp\left[-\frac{v_i/v_p}{(1+0.5\beta C^t \Delta t)}\right]. \quad (25)$$

For the geometric size grid

$$dv_i = 2v_i \frac{V_{RAT}-1}{V_{RAT}+1}. \quad (26)$$

To compare solutions, we used the same initial number concentration and coagulation kernel as in the previous examples. Also, the peak volume diameter was 0.1 μm while the time-step and total coagulation period were 600 s and 12 h, respectively. Figure 4 shows results when $V_{RAT} = 1.5$ and $V_{RAT} = 2$. The

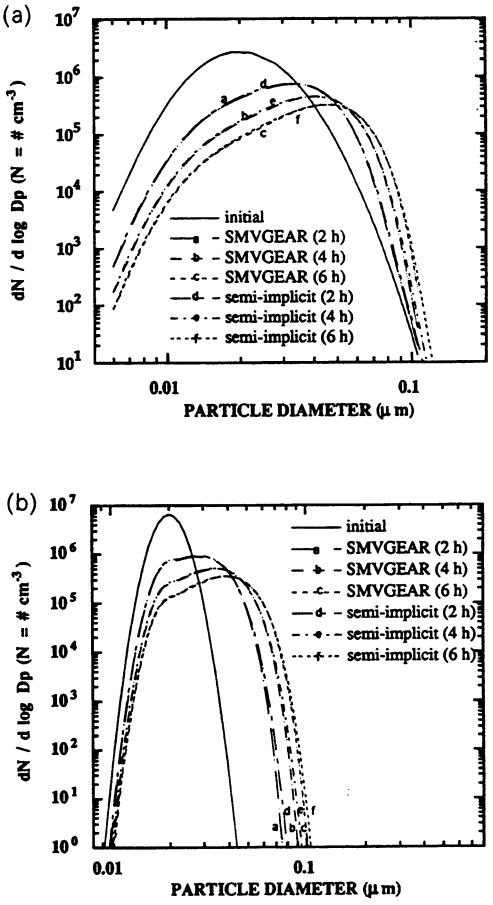

Fig. 3. Comparisons of semi-implicit to integrated coagulation results when the initial distributions were lognormal. The initial mean number diameter and concentration in both figures were 0.02 μm and 10^6 cm^{-3}, respectively. The initial geometric standard deviation was 1.4 in Fig. 3a and 1.15 in Fig. 3b. The coagulation kernel was constant and the same as in Example 1. The coagulation period was 6 h, with results shown every 2 h. For each of the semi-implicit cases, V_{RAT} was 1.2 and the time-step was 600 s. We used SMVGEAR to solve equation (2) over 5500 monomer size-bins (5500 equations and unknowns) for Fig. 3a and 2000 bins for Fig. 3b.

semi-implicit solution followed the analytical solution except at large sizes, where numerical diffusion caused some error. However, with decreasing V_{RAT}, numerical diffusion decreased while with a smaller or larger time-step (not shown), the results changed insignificantly.

In the fifth test we compared the semi-implicit scheme to results from the continuous representation, J-space transformation model (COAGUL) of Suck and Brock (1979), as shown in Seigneur *et al.* (1986). The aerosol tested was uniform in composition and had an initial tri-modal distribution with mean volume diameters of 0.038, 0.32, and 5.7 μm, geometric standard deviations of 1.8, 2.16, and 2.21, and volumes of 0.63, 38.4, and 30.8 μm^3 cm^{-3}, respectively, in each mode (data from Whitby, 1978). The only coagulation rate term used was that for Brownian coagulation

(equation (29)). Figure 5 shows results of the comparison after 12 h of simulated coagulation. The semi-implicit model predicted the aerosol distribution similarly to that of COAGUL. Furthermore, semi-implicit coagulation conserved volume exactly, decreased the number density of particles, and moved particles to larger sizes. Because this was a model to model comparison, it is difficult to determine the extent of numerical diffusion.

5. APPLICATION OF THE ALGORITHM

Here, we apply the semi-implicit model to a multicomponent set of aerosols and concentrations that could exist in an automobile tunnel. The purpose of the demonstration is to show the features, speed, and volume conservation of our mechanism and to suggest that pure particles quickly coagulate to become mixed particles in a particle-rich environment. The only process included in this simulation was coagulation.

For the example, we used the species and conditions listed in Table 2. For modeling purposes, we separated elemental and organic carbon into separate EM types with one component each, constructed the organic carbon size distribution different from that of elemental carbon, and put no initial carbon in IM particles. Elemental carbon and other particles are not spherical in reality; however, we modeled them as such for simplicity. Because the semi-implicit model is independent of the size-bin structure, it can coagulate particles of odd shapes so long as the kernel is modified and average particle shapes are known.

Among the data we used were size-resolved elemental carbon data gathered from the Caldecott Tunnel (Venkatram, 1992). We also assumed that the ratio of elemental to organic carbon particle concentrations in the tunnel was 1.4 (Hering *et al.*, 1984). Finally, we fit lognormal distributions to all carbon data.

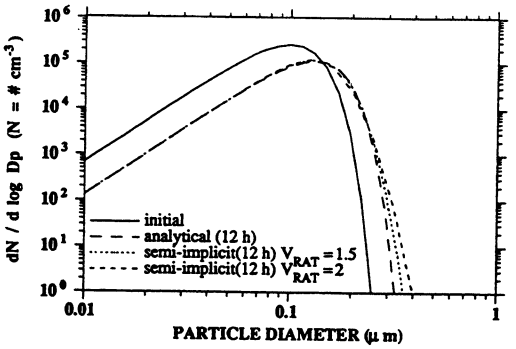

Fig. 4. Comparison of semi-implicit coagulation results to the analytical solution of equation (25). The coagulation period was 12 h, the initial distribution centered about a peak at 0.1 μm diameter, and the coagulation kernel was constant. The figure shows semi-implicit solutions for $V_{RAT}=1.5$ and $V_{RAT}=2$. The time-step for the semi-implicit method was 600 s.

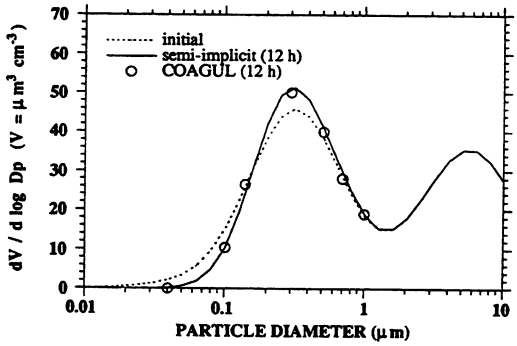

Fig. 5. Comparison of results from the semi-implicit scheme to those of COAGUL (Suck and Brock, 1979—results shown in Seigneur *et al.*, 1986). The coagulation period was 12 h, the initial distribution was tri-modal (Whitby, 1978), and the kernel was that for Brownian motion only. For the semi-implicit model, $\Delta t=600$ s, $V_{RAT}=2$, $r_1=0.005$ μm, and $N_B=40$.

Table 2. Initial distribution of IM and EM aerosols. The distributions of each are the sum of their volume fraction distributions. D_{gv} is the geometric mean volume diameter and σ_g is the geometric standard deviation of each mode

	Nuclei mode			Accumulation mode			Coarse mode		
Particle	Mass (μg m^{-3})	D_{gv} (μm)	σ_g	Mass (μg m^{-3})	D_{gv} (μm)	σ_g	Mass (μg m^{-3})	D_{gv} (μm)	σ_g
1. EM1									
1a. Elemental C	67	0.107	1.66	0	0	0	0	0	0
2. EM2									
2a. Organic C	47.6	0.136	1.50	0	0	0	0	0	0
3. EM3									
3a. Sulfate	0.008	0.04	1.8	0.49	0.32	2.16	0.05	12.3	2.4
3b. Water	0.012	0.04	1.8	0.74	0.32	2.16	0.075	12.3	2.4
4. IM									
4a. Elemental C	0	0	0	0	0	0	0	0	0
4b. Organic C	0	0	0	0	0	0	0	0	0
4c. Sulfate	0.072	0.04	1.8	4.43	0.32	2.16	0.45	12.3	2.4
4d. Water	0.1	0.04	1.8	5.00	0.32	2.16	2.0	12.3	2.4
4e. Nitrate	0.003	0.04	1.8	2.0	0.32	2.16	2.5	8.1	2.4

Because vehicles emit little sulfur, we assumed sulfate entered the tunnel with other background material. For modeling purposes, we placed about 90% of initial sulfate in IM particles and 10% in EM particles. We assumed the sulfate distributions were tri-modal and used the *urban average* geometric mean volume diameter and standard deviation from Whitby (1978) for the nuclei and accumulation modes. We also assumed a nuclei plus accumulation mode sulfate mass of 5.0 $\mu g\,m^{-3}$ and distributed the mass among these two modes and the IM and EM types. For the coarse mode of sulfate, we used a size and mass distribution from Noll *et al.* (1990).

Finally, we distributed nitrate in the IM type using a tri-modal distribution. For the coarse mode, we used a size and mass distribution from Noll *et al.* (1990). For the other modes, we used the same distribution as for sulfate, but set a smaller mass loading. Nitrate was the only species in the IM type which did not also appear in an EM type.

Figure 6 shows the initial and final sum of the volume distributions of the four particle types we coagulated for this application. Coagulation of four types behaved similarly to self-coagulation of a single type containing the same initial distribution as the sum of the four separate distributions. The figure also shows that coagulation affected the size distribution of particles primarily less than one micron in diameter.

By summing all volumes in EM and IM particles before and after coagulation, we found that the semi-implicit mechanism exactly conserved volume. Furthermore, by summing the volume of each EM type and its IMVF counterpart, both before and after coagulation, we found that heterogeneous coagulation exactly conserved volume.

Figure 7 shows the individual changes in EM and IM particle size distributions. Many EM particles hetero-coagulated to become IM particles. Since most initial particles were small, most accumulation of IM particles occurred at sub-micron sizes.

Figures 8 and 9 show the initial and final distribution and composition, respectively, of the IM type. Initially, IM particles contained only sulfate, nitrate

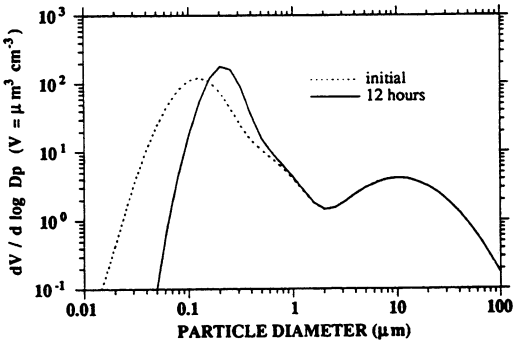

Fig. 6. Volume distribution of the sum of EM and IM particle distributions before and after 12 h of coagulation. Coagulation moved the sum of the distribution of small particles towards larger sizes. Large particles tended to coagulate with much smaller particles, hardly affecting the total volume distribution of the large particles. While the sum of the coarse volume distributions changed little, the distribution of individual particle types changed dramatically (Figs 7–9).

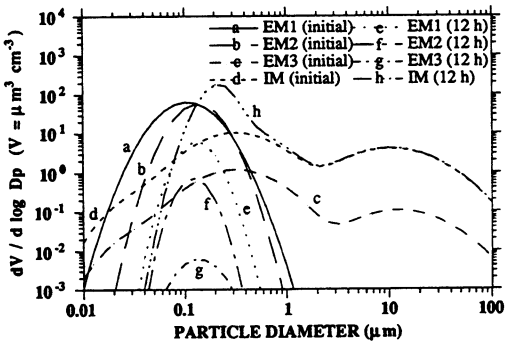

Fig. 7. Change in volume distributions due to 12 h of coagulation. EM1 is elemental carbon, EM2 is organic carbon, EM3 is the sulfuric acid–water mixture, and IM is the internally mixed type. Most volume shifted from EM to IM particles. Addition to the IM coarse mode is hardly noticeable since few large particles existed initially, and they usually coagulated with small particles.

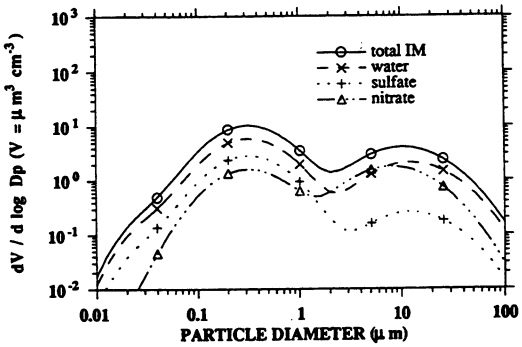

Fig. 8. Initial composition and size distribution of IM particles. IM particles initially consisted of water, sulfate, and nitrate, but no elemental or organic carbon. *Total IM* is the sum of the volumes of water, sulfate, and nitrate. Table A.2 details the initial distributions.

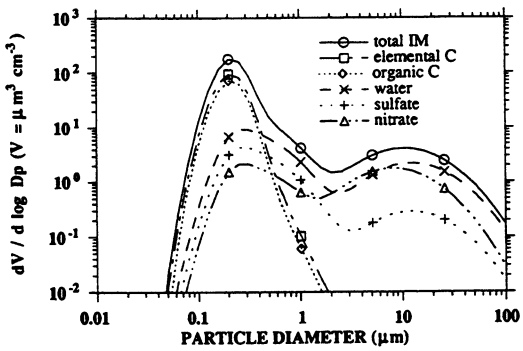

Fig. 9. Composition and size distribution of IM particles after 12 h of coagulation. *Total IM* is the sum of the volumes of elemental and organic carbon, water, sulfate, and nitrate. Coagulation moved a significant amount of elemental and organic carbon from EM to IM particles.

and water, in small amounts. Subsequently, significant amounts of carbon coagulated with and became part of IM particles, drowning out other sub-micron components.

To obtain the computer results for this application, we used 72 600-s time-steps for a total of 12 h. Also, we set $V_{RAT}=2$, $r_1=0.005$ μm, $N_B=41$, and $T=298$ K. The 12-h simulation over one spatial grid-cell took 1.25 s of CPU time on a CRAY Y-MP. Because we vectorized the coagulation code over the grid-cell dimension, increasing the number of grid-cells decreases the time to solve per grid-cell. For example, the same solution, over 16,000 grid-cells, took 571 s at a speed of 209 megaflops. Since we used 41 size bins, 11 distinct aerosol components, and 72 time-steps, the required time was 1.1×10^{-6} s per grid-cell per size bin per component per time-step.

In another coagulation example, not shown here, we ran a simulation with the same 600-s time-step and 12-h interval, but with 6 components and 18 size bins. Over a 16,000-cell grid domain, the solution took 126.4 s at a speed of 205 megaflops. Thus the time required was 1.0×10^{-6} s per grid-cell per size bin per component per time-step, similar to the time in the example above.

6. CONCLUSION

We have presented a model to compute coagulation among any number of particle types, each containing any number of components. The scheme is volume conserving and unconditionally stable, uses any time-step, and solves over any size-bin structure. With a geometric distribution as described in this paper, the scheme can solve for all cases where the volume ratio of adjacent bins (V_{RAT}) exceeds one. The solution mechanism discussed is an expansion of the semi-implicit numerical schemes of Turco *et al.* (1979a,b) and Toon *et al.* (1988). Because the code requires no iterations, it uses little computer time. With the model, we can study effects of coagulation on particle composition and size-distribution. For example, we can simulate coagulation of particles of the same size but of different composition.

The equations shown for multiple particle types assume that whenever a particle of one type coagulates with a particle of another type, the resulting particle enters a multicomponent mixture representing all particle types. In reality, hetero-coagulation results in unique types. We discussed a straightforward method of modifying the equations to account for all possible particle combinations. However, including all combinations drastically increases the number of aerosol constituents. Beyond a small number of spatial grid-cells, aerosol components, and size bins, assuming unique particle types upon hetero-coagulation presses most computer memory limits.

In this paper, we compared results to two analytical solutions, two time-series numerical solutions, and a published solution. In all comparisons, the results matched very well with $V_{RAT}=1.2$ and reasonably well with $V_{RAT}=1.5$–2.0. With larger values of V_{RAT}, numerical diffusion increased at larger size bins. Finally, we demonstrated the use of the model in a slightly more complicated application. The results of the application suggest that single component particles quickly hetero-coagulate with particles of other types when the air is particle-rich. Along with coagulation, however, other processes—such as growth, evaporation, nucleation, deposition, advection, chemical reaction, and emissions — affect aerosol size and composition. Thus, calculating the effects of all processes, not just of coagulation, is important for simulating particle size and composition.

Acknowledgements—We thank the Environmental Protection Agency for support under grant CR-812771-03-0 and the National Science Foundation for partial support under grant A7M-89-11836. We also thank NAS computer center at NASA Ames Research Center, Mountain View, California for permitting our use of a CRAY Y-MP computer.

REFERENCES

Friedlander S. K. (1983) Dynamics of aerosol formation by chemical reaction. *Ann. NY Acad. Sci.* **404,** 354–364.

Fuchs N. A. (1964) *The Mechanics of Aerosols* (translated by Daisley R. E. and Fuchs M.). Pergamon Press, New York.

Gelbard F. and Seinfeld J. H. (1980) Simulation of multicomponent aerosol dynamics. *J. Colloid interf. Sci.* **78,** 485–501.

Hidy G. M. and Brock J. R. (1970) *The Dynamics of Aerocolloidal Systems*, chapter 9. Pergamon Press, Oxford.

Hirschfelder J., Curtiss J. and Bird R. (1951) *Molecular Theory of Gases and Liquids.* John Wiley, New York.

Jacobson M. Z. and Turco R. P. (1994) SMVGEAR: a sparse-matrix, vectorized Gear code for Atmospheric models. *Atmospheric Environment* **28,** 273–284.

Kasten F. (1968) Falling speed of aerosol particles. *J. appl. Met.* **7,** 944–947.

Kim Y. P. and Seinfeld J. H. (1990) Numerical solution of the multicomponent aerosol general dynamic equation. In *Proc. 3rd Int. Aerosol Conf., Science, Industry, Health and Environment*, pp. 138–141. Pergamon Press, Oxford.

Lushnikov A. A. (1975) Evolution of coagulating systems. *J. Colloid interf Sci.* **54,** 94–101.

Main H. H. and Friedlander S. K. (1990) Dry deposition of atmospheric aerosols by dual tracer method — I. Area source. *Atmospheric Environment* **24A,** 103–108.

Millikan R. A. (1923) The general law of fall of a small spherical body through a gas, and its bearing upon the nature of molecular reflection from surfaces. *Phys. Rev.* **22,** 1.

Muller H (1928) *Kolloidbeihefte* **27,** 223.

Noll K. E., Fang K. Y. P. and Khalili E. (1990) Characterization of atmospheric coarse particles in the Los Angeles basin. *Aerosol Sci. Technol.* **12,** 28–38.

Ouimette J. J. and Flagan R. C. (1982) The extinction coefficient of multicomponent aerosols. *Atmospheric Environment* **16,** 2405–2419.

Pruppacher H. R. and Klett J. D. (1978) *Microphysics of Clouds and Precipitation.* D. Reidel, The Netherlands.

Saffman, P. G. and Turner J. S. (1956) On the collision of drops in turbulent clouds. *J. Fluid Mech.* **1,** 16–30.

Seigneur C. (1982) A model of sulfate aerosol dynamics in atmospheric plumes. *Atmospheric Environment* **16,** 2207–2228.

Seigneur C., Hudischewskyj A. B., Seinfeld J. H., Whitby K. T., Whitby E. R., Brock J. R. and Barnes H. M. (1986) Simulation of aerosol dynamics: a comparative review of mathematical models. *Aerosol Sci. Technol.* **5**, 205–222.

Seinfeld J. H. (1986) *Atmospheric Chemistry and Physics of Air Pollution.* John Wiley, New York.

Sitarski M. and Seinfeld J. H. (1977) Brownian coagulation in the transition regime. *J. Colloid interf. Sci.* **61**, 261–271.

Smoluchowski M. V. (1918) Versuch einer mathematischen Theorie der Koagulationskinetik kolloider Losungen. *Z. Phys. Chem.* **92**, 144.

Strom J., Okada K. and Heintzenber J. (1992) On the state of mixing of particles due to Brownian coagulation. *J. Aerosol Sci.* **23**, 467–480.

Suck S. H. and Brock J. R. (1979) Evolution of atmospheric aerosol particle size distributions via Brownian coagulation: numerical simulation. *J. Aerosol Sci.* **10**, 581–590.

Toon O. B., Turco R. P., Westphal D., Malone R. and Liu M. S. (1988) A multidimensional model for aerosols: description of computational analogs. *J. atmos. Sci.* **45**, 2123–2143.

Tsang T. H. and Brock J. R. (1982) Aerosol coagulation in the plume from a cross-wind line source. *Atmospheric Environment* **16**, 2229–2235.

Turco R. P., Hamill P., Toon O. B., Whitten R. C. and Kiang C. S. (1979a) A one-dimensional model describing aerosol formation and evolution in the stratosphere. Part I: Physical processes and mathematical analogs. *J. atmos. Sci.* **36**, 699–717.

Turco R. P., Hamill P., Toon O. B., Whitten R. C. and Kiang C. S. (1979b) The NASA-Ames Research Center stratospheric aerosol model: I physical processes and computational analogs. NASA Tech. Publ. (TP) 1362, iii-94.

Venkatram C. (1992) Polycyclic aromatic hydrocarbon and elemental carbon size distributions in Los Angeles aerosol: source resolution and deposition velocities. Ph.D. thesis, Department of Chemical Engineering, University of California, Los Angeles.

Waggoner A. P., Weiss R. E., Ahlquist N. C., Covert D. S., Will S. and Charlson R. J. (1981) Optical characteristics of atmospheric aerosols. *Atmospheric Environment* **15**, 1891–1909.

Warren D. R. and Seinfeld J. H. (1985) Simulation of aerosol size distribution evolution in systems with simultaneous nucleation, condensation, and coagulation. *Aerosol Sci. Technol.* **4**, 31–43.

Whitby K. T. (1978) The physical characteristics of sulfur aerosols. *Atmospheric Environment* **12**, 135–159.

APPENDIX

Table A.1. Example set of aerosols used to describe coagulation among particles of different size and composition. EM, externally mixed particles; EMVFs, volume fractions of EM particles; IM, internally mixed particles; and IMVF, volume fraction of IM particles

Aerosol No.	Description of type
1	EM1 (made of EMVF1a)
2	EMVF1a (only volume fraction of EM1)
3	EM2 (made of EMVF2a and EMVF2b)
4	EMVF2a (first volume fraction of EM2)
5	EMVF2b (second volume fraction of EM2)
6	IM (made of IMVFa-f)
7	IMVFa (contains same material type as EMVF1a)
8	IMVFb (contains same material type as EMVF2a)
9	IMVFc (contains same material type as EMVF2b)
10	IMVFd (appears only in IM)
11	IMVFe (appears only in IM)
12	IMVFf (appears only in IM)

Parameter definitions as applied to Table A.1.

N_B total number of aerosol size bins

N_T total number of aerosol types (EM plus IM). Does not include volume fractions ($N_T=3$ in Table A.1)

N_E total number of EM types ($N_E=N_T-1=2$ in Table A.1)

V_N total number of volume fractions of each $N=1$, N_T aerosol type ($V_1=1$, $V_2=2$, $V_3=6$ in Table A.1)

T_N total number of components of each $N=1$, N_T aerosol type. $T_N=1+V_N$. In Table A.1, $T_1=2$, $T_2=3$, and $T_3=7$

$L_{N,U}$ aerosol number of each $U=1$, T_N component of each $N=1$, N_T aerosol type. Table A.2 lists example values resulting from Table A.1

$S_{Q,I}$ aerosol number mapping each $Q=L_{N,U}$ IM component to each EM component that hetero-coagulates to form a portion of Q. Table A.2 lists example values resulting from Table A.1

$C^t_{L_{N,}j}$ {Total number concentration of particles of type N, size $j=\sum_{m=1}^{V_N} C^t_{L_{N,m+1},j}$.} Since all concentrations, including those of volume components, are in units of No. cm^{-3}, the sum of the *number concentrations* of all volume fractions of type N, size j equals the total number concentration of particles of that type and size. Similarly, the total volume of a particle (cm^3 $particle^{-1}$) multiplied by the number concentration of one of its volume fractions equals the volume concentration (cm^3 cm^{-3}) of the volume fraction.

Table A.2. Arrays of species number for the parameters $L_{N,U}$ and $S_{Q,M}$. N varies from 1 to $N_{T,U}$, U varies from 1 to T_N, and N_E. The values apply to Table A.1

	←$N=1$→		←$N=2$→			←$N=3$→						
U	1	2	1	2	3	1	2	3	4	5	6	7
$Q=L_{N,U}$	1	2	3	4	5	6	7	8	9	10	11	12
	←$S_{Q,I}$→											
$I=1$	0	0	0	0	0	1	2	0	0	0	0	0
$I=2$	0	0	0	0	0	3	0	4	5	0	0	0